Reprogramming the microenvironment with tumor-selective angiotensin blockers enhances cancer immunotherapy

Vikash P. Chauhan[a,b,c,1], Ivy X. Chen[a,b,c,1], Rong Tong[b,d,e,f,1], Mei Rosa Ng[a], John D. Martin[a,g], Kamila Naxerova[h], Michelle W. Wu[a], Peigen Huang[a], Yves Boucher[a], Daniel S. Kohane[d,e,f], Robert Langer[b,g,2], and Rakesh K. Jain[a,2]

[a]Edwin L. Steele Laboratories, Department of Radiation Oncology, Massachusetts General Hospital, Harvard Medical School, Boston, MA 02114; [b]Koch Institute for Integrative Cancer Research, Massachusetts Institute of Technology, Cambridge, MA 02139 ; [c]Harvard School of Engineering and Applied Sciences, Harvard University, Cambridge, MA 02138; [d]Laboratory for Biomaterials and Drug Delivery, Boston Children's Hospital, Harvard Medical School, Boston, MA 02115; [e]Department of Anesthesiology, Boston Children's Hospital, Harvard Medical School, Boston, MA 02115; [f]Division of Critical Care Medicine, Boston Children's Hospital, Harvard Medical School, Boston, MA 02115; [g]Department of Chemical Engineering, Massachusetts Institute of Technology, Cambridge, MA 02139; and [h]Center for Systems Biology, Massachusetts General Hospital, Harvard Medical School, Boston, MA 02114

Contributed by Robert Langer, April 1, 2019 (sent for review November 27, 2018; reviewed by David Putnam and W. Mark Saltzman)

Cancer-associated fibroblasts (CAFs) can either suppress or support T lymphocyte activity, suggesting that CAFs may be reprogrammable to an immunosupportive state. Angiotensin receptor blockers (ARBs) convert myofibroblast CAFs to a quiescent state, but whether ARBs can reprogram CAFs to promote T lymphocyte activity and enhance immunotherapy is unknown. Moreover, ARB doses are limited by systemic adverse effects such as hypotension due to the importance of angiotensin signaling outside tumors. To enhance the efficacy and specificity of ARBs in cancer with the goal of revealing their effects on antitumor immunity, we developed ARB nanoconjugates that preferentially accumulate and act in tumors. We created a diverse library of hundreds of acid-degradable polymers and chemically linked ARBs to the polymer most sensitive to tumor pH. These tumor microenvironment-activated ARBs (TMA-ARBs) remain intact and inactive in circulation while achieving high concentrations in tumors, wherein they break down to active ARBs. This tumor-preferential activity enhances the CAF-reprogramming effects of ARBs while eliminating blood pressure-lowering effects. Notably, TMA-ARBs alleviate immunosuppression and improve T lymphocyte activity, enabling dramatically improved responses to immune-checkpoint blockers in mice with primary as well as metastatic breast cancer.

drug delivery | tumor microenvironment | cancer immunotherapy

Immunotherapy using checkpoint blockers has revolutionized the treatment of melanoma, lung, head and neck, bladder, and colorectal cancers (1). However, a similar impact has yet to be seen in other solid tumors. A hallmark of some nonresponsive tumors, such as desmoplastic breast cancers, is that they are rich in cancer-associated fibroblasts (CAFs) and extracellular matrix (2). CAFs exist in a variety of states that can be either immunosuppressive or immunosupportive (3). Immunosuppressive CAFs hinder antitumor immunity through secreted factors such as CXCL12 and CXCL13 (3–7). These CAFs, which are a subset of myofibroblast-type α-smooth-muscle actin (αSMA+) cells that may express FAP, can exclude cytotoxic T lymphocytes from tumors while attracting immunosuppressive regulatory T lymphocytes or B lymphocytes (3–6). The dense collagen matrix produced by αSMA+ CAFs may also present a physical barrier to the infiltration of T lymphocytes (8). Furthermore, mechanical compression of tumor blood vessels through buildup of physical pressure, termed solid stress, by αSMA+ CAFs and matrix leads to tissue hypoxia and low pH (9–11). Hypoxia and/or low pH can promote T regulatory cell activity, increase expression of the immune checkpoint protein programmed death-ligand 1 (PD-L1), and suppress the activity of T lymphocytes (12–15). Thus, a subset of myofibroblast-type CAFs and the matrix they generate promote multifaceted immunosuppression.

Therapeutic means for eliminating CAF-driven protumor effects remain elusive. Reducing the population of activated CAFs would seem appealing, but genetic depletion of all αSMA+ cells hinders the immune response and promotes cancer progression (16). This may be a result of the loss of all myofibroblast-type CAFs, including immunosupportive CAFs as well as CAF precursors and related cells such as quiescent fibroblasts, stellate cells, and pericytes that have critical roles in tissue homeostasis (17, 18). In contrast, genetic depletion of only FAP+ CAFs can support antitumor immunity and limit cancer growth (4, 5). Thus, it is possible to boost antitumor immunity by depleting a subset of CAFs, although there are limited therapeutic options for doing so. The fact that there are immunosuppressive and immunosupportive subsets of myofibroblast-type αSMA+ CAFs

Significance

Cancer-associated fibroblasts (CAFs) can either inhibit or enable antitumor immunity, suggesting that they may be reprogrammed between these states. Angiotensin receptor blocker (ARB) drugs can reprogram CAFs to a quiescent state, but it is not known whether ARBs can enhance immune responses to cancer. Moreover, angiotensin signaling drives other important physiological processes and ARBs cause systemic adverse effects that limit their use in cancer. Here we created safer ARBs by chemically linking them to a polymer that degrades selectively in the slightly acidic microenvironment of solid tumors but not in the neutral environment outside of tumors. This tumor selectivity makes ARBs more effective at reprogramming CAFs while eliminating their side effects. These enhanced ARBs reduce immunosuppression and improve cancer immunotherapy efficacy.

Author contributions: V.P.C., I.X.C., R.T., R.L., and R.K.J. designed research; V.P.C., I.X.C., R.T., M.R.N., and M.W.W. performed research; V.P.C., I.X.C., and R.T. contributed new reagents/analytic tools; V.P.C., I.X.C., R.T., M.R.N., J.D.M., K.N., P.H., Y.B., D.S.K., R.L., and R.K.J. analyzed data; and V.P.C., I.X.C., R.T., R.L., and R.K.J. wrote the paper.

Reviewers: D.P., Cornell University; and W.M.S., Yale University.

Conflict of interest statement: Massachusetts General Hospital and the Massachusetts Institute of Technology have applied for a patent based on this work. A full list of all financial interests is included in *SI Appendix*.

Data deposition: The data reported in this paper have been deposited in the Gene Expression Omnibus (GEO) database, https://www.ncbi.nlm.nih.gov/geo (accession no. GSE98827).

[1]V.P.C., I.X.C., and R.T. contributed equally to this work.

[2]To whom correspondence may be addressed. Email: rlanger@mit.edu or jain@steele.mgh.harvard.edu.

This article contains supporting information online at www.pnas.org/lookup/suppl/doi:10.1073/pnas.1819889116/-/DCSupplemental.

Published online April 30, 2019.

suggests that CAFs may be reprogrammed between these states. Indeed, CAFs have been shown to be reprogrammable from active to quiescent myofibroblast states, for example by blocking signaling that promotes myofibroblast activity such as angiotensin II (AngII) signaling through AngII receptor type-1 (AT1) (10) or by modulating master transcriptional regulators of myofibroblast phenotype such as vitamin D receptor (17). Agents such as angiotensin receptor blockers (ARBs), which block AngII signaling, inactivate the myofibroblast state of CAFs and reduce αSMA+ CAF levels (10). However, because αSMA+ CAFs may be either immunosuppressive or immunosupportive, it remains unknown how these CAF-reprogramming effects of ARBs will affect antitumor immunity.

The nature of these therapeutics poses an additional challenge to identifying their effects on the tumor microenvironment. ARBs and other CAF-reprogramming agents were not designed for use in cancer. Targeting CAF signaling carries risks inherent in the importance of these signaling pathways in normal physiological processes. AngII/AT1 signaling, for example, regulates blood pressure, and the ARBs that inhibit this signaling can induce hypotension and CAF reprogramming with similar potency (19). As a result, these therapies can only be applied at limited doses in cancer. Accordingly, an early clinical trial of ARBs in advanced pancreatic cancer showed moderate anticancer efficacy only at doses that caused hypotension (20), and a recent trial showed promising results but was limited to nonhypotensive doses of ARBs (21). Thus, it is currently challenging to evaluate the potential benefits of ARBs for antitumor immunity.

To explore whether ARBs could have immunosupportive effects we therefore set out to address these limitations on their effectiveness in the tumor microenvironment. We hypothesized that ARBs could be redesigned for greater efficacy in cancer through modification such that the drugs accumulate and selectively act in tumors. Earlier formulations of ARBs, such as liposomal encapsulations, have not provided this manner of selective activity (22). Thus, we sought to create targeted forms of ARBs that are selectively activated in the tumor microenvironment, or TMA-ARBs. We reasoned that chemically conjugating an ARB to polymers that selectively degrade in the tumor microenvironment would produce an ARB nanoconjugate with the desired tumor specificity, as this would afford ARBs a nanoscale size for improved tumor accumulation and tumor-selective release for localized activity. As a consequence of hypoxia, many solid tumors and their metastases are acidic in comparison with most normal tissues, with pH in the range of 6.7 to 7.2 (23–25), indicating low pH as an attractive trigger for selective activation in tumors. While pH-sensitive materials have been available for nearly four decades (26–28), we aimed to develop materials that are sensitive to the very small difference between physiological and tumor pH.

Results

Design of a Chemically Diverse Library of pH-Sensitive Polymers. We developed a high-throughput combinatorial chemistry approach to create a chemically diverse library of pH-sensitive polymeric materials. We employed modular acetal exchange or polycondensation reactions (29–31) to polymerize polyol and acetal or

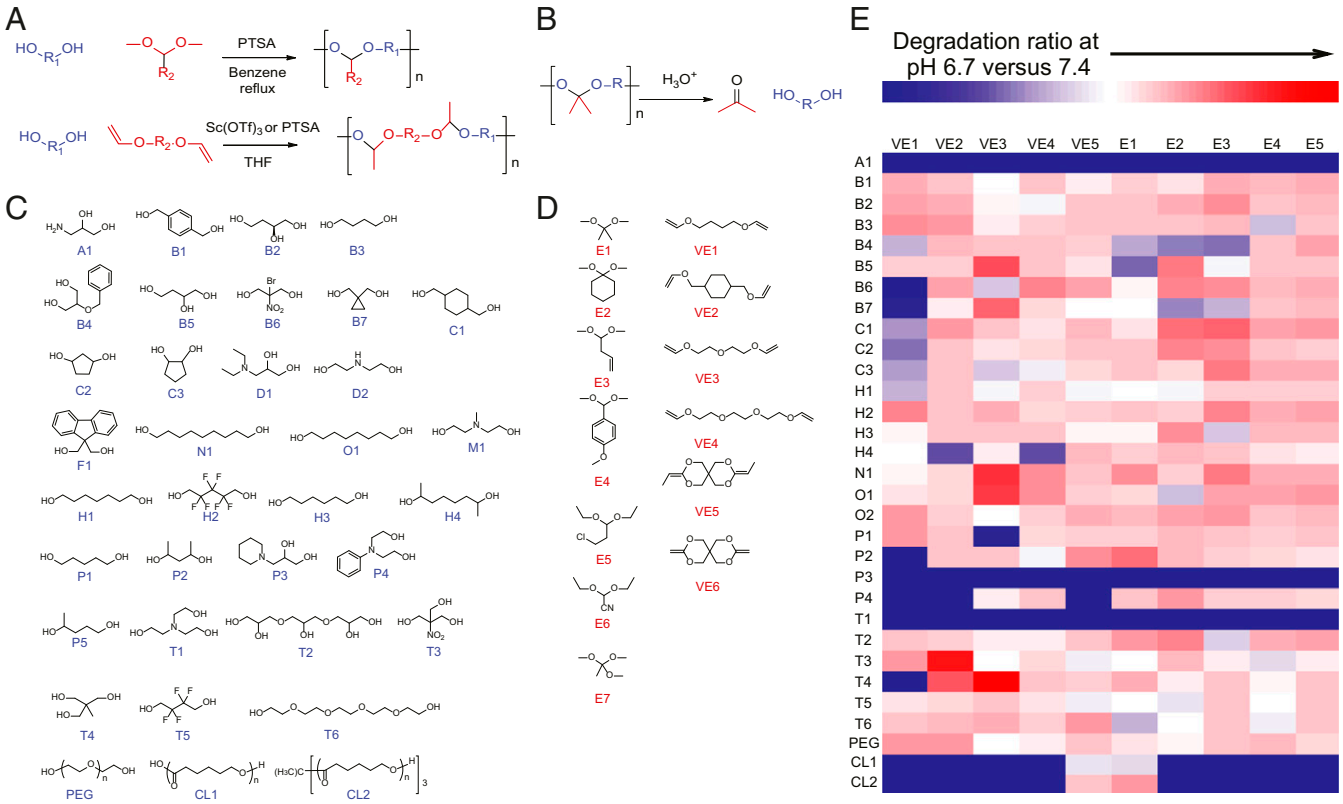

Fig. 1. Synthesis of a diverse library of polymers sensitive to slight acidic shifts. (*A*) Modular acetal exchange (*Top*) and polycondensation (*Bottom*) reactions to polymerize polyol (blue) and acetal or vinyl ether (red) monomers into polyacetals. A diverse set of monomers was used to create 936 unique polyacetals using a high-throughput combinatorial synthesis approach. (*B*) Polyacetal degradation reaction under acidic conditions. (*C*) Set of 36 polyol monomers for polyacetal synthesis. (*D*) Set of seven acetals (*Left*) and six vinyl ethers (*Right*) for polyacetal synthesis. (*E*) High-throughput fluorometric assay of polyacetal pH sensitivity. Each polyacetal was created from the combination of one polyol monomer (A1–CL2) and one acetal (E1–E5) or vinyl ether (VE1–VE5) monomer. Several polymers were highly sensitive to acidic conditions (red).

polyol and vinyl ether monomers, respectively, into polyacetals (Fig. 1*A*), which degrade under acidic conditions (Fig. 1*B*). By combining a set of 36 polyols (Fig. 1*C*) with a set of 7 acetals and 6 vinyl ethers (Fig. 1*D*) using a one-pot synthesis (32, 33), with or without PEG (molecular weight 400 Da or 1 kDa), we created 936 unique polyacetals. We then screened the polymer library by characterizing molecular weights, nanoparticle formulation ability, and pH sensitivity. Screening the polymers rather than polymer–ARB conjugates alleviated the synthetic workload while allowing for identification of useful pH-sensitive polymers. We first eliminated those combinations of monomers that did not produce polymers of molecular weight greater than 1 kDa following polymerization (*SI Appendix*, Fig. S1), reasoning that formation of robust polymers would be essential for nanoparticle formulation. We formulated the remaining polymers into nanoparticles through nanoprecipitation and measured nanoparticle formation using dynamic light scattering, then further eliminated those polymers that did not form nanoparticles with sub-100-nm sizes, which are ideal for tumor penetration (34, 35). To characterize the pH sensitivity of each nanoparticle, we developed a high-throughput fluorometric pH-sensitivity assay based on liberation of Nile Red, whose fluorescence is quenched upon release from the particles into aqueous buffer (Fig. 1*E*). This assay identified several polymers that broke down at tumor pH (6.7) more rapidly than at normal physiological pH (7.4). Through analysis of pH-sensitivity patterns, we found that polymers synthesized from hydrophobic monomers appeared to have insignificant degradation rate differences at pH 6.7 and 7.4; the accessibility of polymer acetal bonds to protons may contribute to acid sensitivity (36). Moreover, we found that the acetals generally hydrolyze more rapidly than the ketals at acidic pH (e.g., E3C1 versus E1C1), whereas ketals from cyclic ketone monomers often exhibit slower hydrolysis rates than those of ketals from acyclic monomers (e.g., E2O1 versus E1O1), similar to recent studies (36). We identified the polyacetal created through reaction of 1,1,1-Tris(hydroxymethyl)ethane (T4) and di(ethylene glycol) divinyl ether (VE3) as the material that degraded most selectively at tumor versus physiological pH.

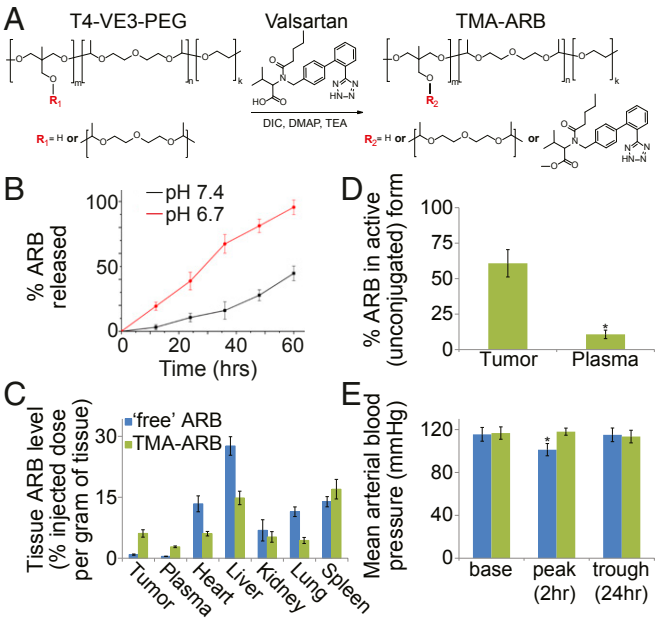

Fig. 2. Conjugation to a pH-sensitive polymer enables tumor targeting of ARBs. (*A*) Reaction for chemical conjugation of an ARB to a polyacetal to create a TMA-ARB. The ARB valsartan and the polyacetal created from T4 and VE3 monomers, which has a branched structure, were used to create a prototype TMA-ARB. (*B*) ARB release from the TMA-ARB under simulated physiological pH (7.4) and tumor pH (6.7) conditions in vitro. $n = 5$. (*C*) Biodistribution of ARB in mice bearing orthotopic MCa-M3C breast tumors 24 h after i.v. injection of the free ARB or the TMA-ARB at equal doses. The TMA-ARB led to tumor ARB levels 6.8-fold higher than levels achieved after injection of the free ARB ($P < 0.01$). $n = 5$–7. (*D*) Fraction of ARB found in its active (unconjugated) versus inactive (conjugated) form in mice injected with the TMA-ARB. The TMA-ARB released ARB to its active form selectively in tumors (*$P < 0.01$). $n = 5$–7. (*E*) Effects of the free ARB and TMA-ARB on MAP in mice. The free ARB reduces MAP by 15 mmHg 2 h after injection, while the TMA-ARB does not affect MAP (*$P = 0.035$). $n = 4$.

TMA-ARBs Selectively Accumulate and Act in Tumors. To produce a prototype TMA-ARB we conjugated the ARB valsartan to this T4–VE3 polyacetal through an ester linkage (Fig. 2*A*). Following conjugation we formulated the TMA-ARB into stable 35-nm nanoparticles (*SI Appendix*, Fig. S2) with acid-sensitive ARB release at pH 6.7 versus 7.4 (Fig. 2*B*). We also generalized this approach to other ARBs (e.g., losartan) using modified synthesis schema (*SI Appendix*, Fig. S3). We next assessed tumor targeting by the TMA-ARB in vivo by measuring the biodistribution of ARB in tumor-bearing mice 24 h following i.v. administration of either the TMA-ARB or an identical dose (equal amount of ARB) of "free" ARB. Administration of the TMA-ARB led to tumor ARB levels (unconjugated and conjugated) nearly sevenfold higher than levels achieved following injection of the free ARB in an orthotopic syngeneic *MMTV-PyVT*–derived MCa-M3C breast cancer model ($P < 0.01$; Fig. 2*C*). The data suggest that these increased tumor levels may be due to slower plasma elimination or greater tumor accumulation for the TMA-ARB. Importantly, 24 h after administration of the TMA-ARB only 10.7% of the total ARB found in plasma was in its unconjugated form, with the remainder still conjugated to the T4–VE3 polymer. Meanwhile, in tumors the TMA-ARB had released 60.8% of the total ARB after 24 h (Fig. 2*D*). We observed similar results in a second cancer model (*SI Appendix*, Fig. S4). To determine if this tumor-selective release has consequences on ARB activity outside tumors, we compared the effects of the TMA-ARB and free ARB on mean arterial blood pressure (MAP). We found that the free ARB reduced MAP by a potentially dangerous 15 mmHg ($P = 0.035$), whereas the TMA-ARB did not affect MAP (Fig. 2*E*). Thus, the tumor microenvironment induces the TMA-ARB to break down and release ARB preferentially at high levels in tumors.

TMA-ARBs Normalize the Tumor Microenvironment to a Greater Degree than Free ARBs. We next assessed whether this enhanced tumor targeting would increase normalization of the tumor microenvironment driven by CAF reprogramming. We treated mice bearing MCa-M3C tumors with the TMA-ARB, an equal dose of free ARB, or an equal volume of saline (control). We measured αSMA and collagen I expression as direct measures of CAF activity, as well as solid stress and vessel compression as consequences of CAF activation (10). TMA-ARB treatment reduced αSMA+ cell density more than free ARB treatment ($P = 0.037$; Fig. 3*A* and *SI Appendix*, Fig. S5). Importantly, these αSMA+ cells include mostly myofibroblast-type CAFs and a small population of other cells such as pericytes. The TMA-ARB also lowered collagen I expression ($P < 0.01$; Fig. 3*B* and *SI Appendix*, Fig. S6) and solid stress levels ($P < 0.01$; Fig. 3*C*) more than the free ARB. By reducing solid stress, the TMA-ARB decompressed tumor blood vessels ($P < 0.01$; Fig. 3*D* and *SI Appendix*, Fig. S7) more than the free ARB without affecting vessel density (Fig. 3*E*), indicating an increase in perfusion. We confirmed these results in a second cancer model (*SI Appendix*, Figs. S6, S8, and S9). The TMA-ARB also improved the outcome of chemotherapy (*SI Appendix*, Figs. S10 and S11), which is known to be hindered by poor perfusion induced by CAF activity (10). Thus, the TMA-ARB alleviates CAF-driven pathologies

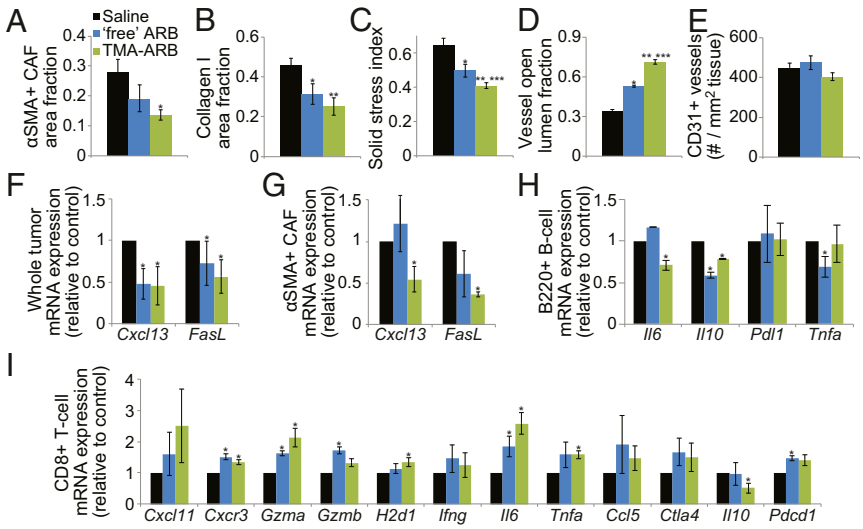

Fig. 3. Tumor-targeted ARBs normalize the tumor microenvironment to a greater degree than free ARBs. (*A–E*) Histological and biomechanical analysis of orthotopic MCa-M3C breast tumors in mice treated with free ARB, TMA-ARB, or saline (control). (*A*) Tumor αSMA+ cell area fractions. TMA-ARB treatment reduced αSMA+ cell (primarily CAF) density (*$P = 0.037$). $n = 6–7$. (*B*) Tumor collagen I area fractions. Both free ARB treatment (*$P = 0.032$) and TMA-ARB treatment (**$P < 0.01$) reduced tumor collagen I expression. $n = 5–8$. (*C*) Relative tumor solid stress levels. Both free ARB treatment (*$P = 0.032$) and TMA-ARB treatment (**$P < 0.01$) reduced solid stress, with the TMA-ARB reducing it more (***$P = 0.05$). $n = 10–11$. (*D*) Fractions of tumor blood vessels with open lumen, indicating the extent of vessel decompression. Both free ARB treatment (*$P < 0.01$) and TMA-ARB treatment (**$P < 0.01$) decompressed blood vessels, with the TMA-ARB most effective (***$P < 0.01$). $n = 4$. (*E*) Tumor blood vessel density. $n = 4$. (*F–I*) Gene expression (qRT-PCR) and cell population (flow cytometry) analysis in whole tumors or cell populations sorted from orthotopic breast tumors in mice treated with free ARB, the TMA-ARB, or saline (control). (*F*) Confirmation of hits from a gene expression array in whole MCa-M3C tumors. Treatment with the ARB decreased *Cxcl13* expression ($P < 0.05$), while treatment with the TMA-ARB decreased *Cxcl13* expression ($P < 0.05$) and *Fasl* expression ($P < 0.05$) in whole tumors. $n = 5–8$. (*G*) Gene expression in αSMA+ cells sorted from E0771 tumors. Treatment with the TMA-ARB decreased *Cxcl13* and *Fasl* expression in these sorted cells ($P < 0.05$). $n = 3–4$. (*H*) Gene expression in CD45+CD3-B220+ B lymphocytes sorted from E0771 tumors. Treatment with the ARB or TMA-ARB decreased expression of genes associated with immunosuppression and autocrine stimulation ($P < 0.05$). $n = 3$. (*I*) Gene expression in CD45+CD3+CD8+ cytotoxic T lymphocytes sorted from E0771 tumors. Treatment with the ARB or TMA-ARB increased expression of several genes associated with cytotoxic T cell activity ($P < 0.05$). $n = 3–4$.

and increases vascular perfusion more than the free ARB at an equal dose.

TMA-ARBs Induce Broad Gene Expression Changes Indicating Reversal of Immunosuppression. To gain a mechanistic molecular-level understanding of the possible effects of TMA-ARB, we carried out RNA sequencing of MCa-M3C breast tumors in mice treated with the TMA-ARB or saline (control). Although few individual genes were differentially expressed (Dataset S1), gene set enrichment analysis identified several pathways in the Hallmarks and Biocarta databases that significantly overlap with differentially expressed genes in our experiment (*SI Appendix*, Fig. S12). Among the top hits, we found that TMA-ARB treatment downregulated hypoxia and TGF-β pathways, consistent with the reductions in vessel compression and CAF activity we observed. TMA-ARB treatment also decreased expression of the Tob1, CTLA4, B cell survival, and inflammatory response pathways, which are related to suppression of the adaptive immune response. While ARBs have been shown to modulate the response of innate immune cells in tumors (37–39), and RNA-sequencing analysis of pancreatic cancer in patients using angiotensin converting enzyme-inhibitors suggests reversal of immunosuppression (40), ARBs have not yet been shown to activate the adaptive immune response to cancer. Since CAFs have been implicated in immunosuppression (4–6), we hypothesized that ARB or TMA-ARB treatment might reprogram the tumor microenvironment into an immunostimulatory milieu.

TMA-ARBs Activate Immunosupportive Pathways in the Immune Microenvironment. To understand potential effects on the immune microenvironment, we analyzed gene expression in MCa-M3C tumors using a cytokine/chemokine expression array and confirmed hits using qRT-PCR (*SI Appendix*, Fig. S13). Treatment with the ARB or TMA-ARB reduced expression of *Cxcl13* and *Fasl* ($P < 0.05$; Fig. 3*F*), which have been implicated in repulsion or exclusion of T lymphocytes by CAFs or vessels (6, 41). CAF expression of CXCL13 is a marker of an immunosuppressive state (3). Moreover, CXCL13 expression by CAFs can be induced by TGF-β and hypoxia signaling (42), which our RNA-sequencing data indicated were decreased by TMA-ARB treatment. To assess whether these immunosuppressive factors changed specifically in CAFs, we sorted CAFs from orthotopic syngeneic E0771 or MCa-M3C breast tumors in treated mice and measured gene expression using qRT-PCR. We confirmed these reductions in *Cxcl13* and *Fasl* expression in sorted CAFs ($P < 0.05$; Fig. 3*G* and *SI Appendix*, Fig. S13), indicating a shift from an immunosuppressive to an immunosupportive state. Since CXCL13 drives immunosuppression through B-lymphocyte recruitment (6) and our RNA-sequencing data indicated that the TMA-ARB inhibited B cell survival and inflammatory response pathways, we also sorted CD45+CD3-B220+ B lymphocytes from E0771 tumors in treated mice and measured gene expression using qRT-PCR. We found that ARB and TMA-ARB treatment decreased expression of *Il10* ($P < 0.05$; Fig. 3*H*), a marker of immunosuppressive B lymphocytes (6).

Considering that our RNA-sequencing data indicated that TMA-ARB treatment decreased Tob1 and CTLA4 signaling, which restrain T lymphocyte activity (1, 43), we also evaluated how TMA-ARB treatment affects the activity of T lymphocytes. We sorted CD45+CD3+CD8+ T lymphocytes from E0771 breast tumors in treated mice and measured gene expression using qRT-PCR. We found that ARB and TMA-ARB treatment increased the expression of several markers of T lymphocyte activation (*Cxcr3*, *Gzma*, *Gzmb*, *H2d1*, *Il6*, and *Tnfa*) while decreasing expression of suppression markers (*Il10*), indicating activation of cytotoxic T lymphocytes ($P < 0.05$; Fig. 3*I*). Since the tumor microenvironment can

also limit T lymphocytes by restricting their intratumoral distribution, particularly through high CAF and collagen density (4, 5, 8, 44), we assessed how ARB treatment affects this distribution. We found that the intratumoral distribution of CD3+ T lymphocytes was augmented with ARB or TMA-ARB treatment, as indicated by a decrease in the distance between CD3+ T lymphocytes and αSMA+ cells (*SI Appendix*, Fig. S14), possibly due to decreases in suppressive signaling by CAFs. Taken together, these data suggest that ARB or TMA-ARB treatment promote a tumor microenvironment that is less suppressive of T lymphocyte activity, likely through decreased hypoxia and TGF-β signaling.

TMA-ARBs Reprogram the Microenvironment and Overcome Resistance to Immunotherapy. Considering that breast cancers are largely nonresponsive to T lymphocyte-mediated immunotherapies (*SI Appendix*, Table S1), we were intrigued by the possibility that the immunostimulatory effects of ARBs might overcome resistance to immune checkpoint blockers. We therefore combined the free ARB or TMA-ARB with a mixture of blocking antibodies against the immune checkpoints cytotoxic T lymphocyte-associated protein 4 (α-CTLA-4) and programmed cell death 1 (α-PD-1) to treat mice bearing E0771 tumors. We found that the free ARB did not improve tumor growth delay when combined with the immune checkpoint blocker mixture, while the TMA-ARB combination with the immune checkpoint blocker greatly enhanced growth delay (*SI Appendix*, Fig. S15). Since the TMA-ARB was superior to free ARB in reprogramming the tumor microenvironment and enhancing immunotherapy, we further studied the effects of the TMA-ARB combination. Using flow cytometry in treated E0771 tumors, we found that TMA-ARB treatment alone increased the number of CD45+ cells (leukocytes), increased the ratio of CD8+ (cytotoxic T lymphocyte) to CD4+CD25+FoxP3+ (regulatory T lymphocyte) cells, increased the ratio of MHCII+ (M1-like, antitumor) to CD206+ (M2-like, protumor) macrophages, increased the number of CD11b+CD11c+ (dendritic) cells, and decreased suppressive TGF-β expression in CD8+ cells (*SI Appendix*, Figs. S16–S18). These data further suggest a reversal of immunosuppression by ARBs. While the immune checkpoint blocker mixture alone also induced recruitment of leukocytes, particularly CD8+ and CD4+ T lymphocytes, and activation of CD8+ T lymphocytes as consistent with previous reports (45, 46), the combination of the TMA-ARB with the immune checkpoint blocker mixture also reduced CD8+ T lymphocyte PD-1 expression [a marker of dysfunction (47)] and generally showed greater immunostimulatory effects than either treatment alone (*SI Appendix*, Figs. S16–S18).

TMA-ARBs Improve the Efficacy of Immune Checkpoint Blockers in Primary Tumors. We next asked whether the immunostimulatory effects of the TMA-ARB would translate to improved outcomes when used in combination with immune checkpoint blockers. We first assessed how these therapies affected tumor growth of the breast cancer models E0771, MCa-M3C, and 4T1 in the primary (orthotopic) setting in syngeneic mice (Fig. 4 *A*–*C*). We found that TMA-ARB monotherapy had no effect on tumor growth. Meanwhile, the immune checkpoint mixture of α-CTLA4 + α-PD-1 resulted in tumor regression with a response rate of 33% for E0771 while it caused no growth delay in MCa-M3C or 4T1 tumors, and all responding tumors eventually relapsed. Combining the TMA-ARB with the immune checkpoint mixture caused regression with a response rate of 66% for E0771 and greatly delayed growth of MCa-M3C by 58% ($P < 0.01$) and 4T1 by 77% ($P < 0.01$), with a 50% cure (complete response) rate for E0771. While it has been reported that this immune checkpoint blocker mixture can induce significant toxic effects (48), only a trend toward higher ALT levels was observed for the immunotherapy treatments and none of these treatments or combinations induced significant toxic effects (*SI Appendix*, Figs. S19–S21 and Table S2). These data indicate that blocking AngII/AT1 signaling and reducing CAF activity with the TMA-ARB can both increase the response rate to immunotherapy and hinder cancer progression further.

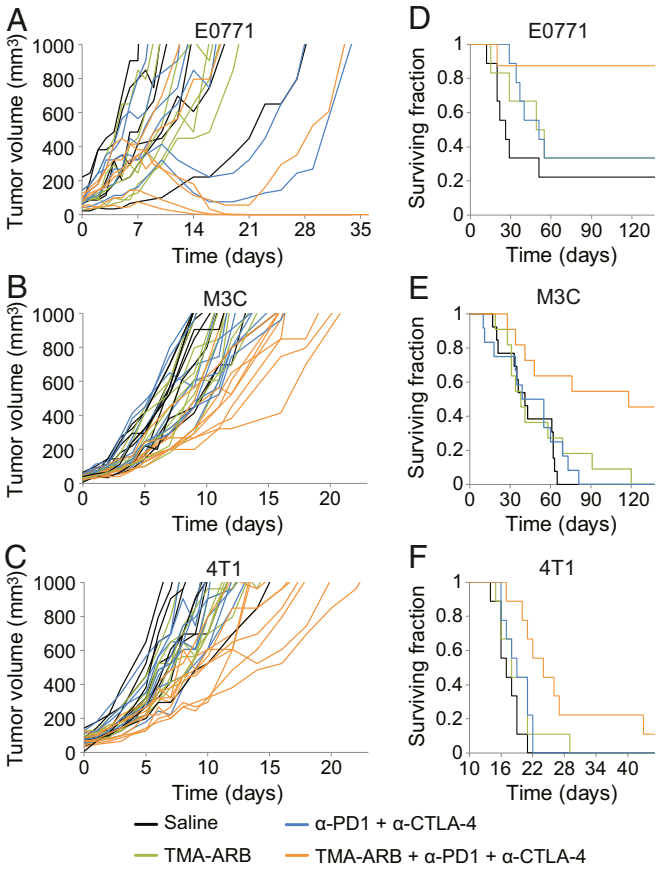

Fig. 4. Tumor-targeted ARBs enhance the outcome of immune checkpoint blockers. (*A*–*C*) Primary tumor growth studies in mice bearing orthotopic breast tumors treated with immune checkpoint blockers in combination with TMA-ARBs. Mice were treated with the TMA-ARB or saline (control) on days 0 to 7, and with or without a mixture of immune checkpoint blocking antibodies against cytotoxic T lymphocyte-associated protein 4 (α-CTLA-4) and programmed cell death 1 (α-PD-1) on days 2, 5, and 8. (*A*) Tumor growth in mice bearing E0771 tumors. The immunotherapy mixture alone cause regression in 2 of 6 tumors, while the combination with the TMA-ARB caused four of six to regress and cured three of six mice. $n = 6$. (*B*) Tumor growth in mice bearing MCa-M3C tumors. The immunotherapy mixture had no effect on tumor growth, while the combination with the TMA-ARB increased the time to reach 1,000 mm^3 by 58%, from 11 to 17 d ($P < 0.01$). $n = 9$–10. (*C*) Tumor growth in mice bearing 4T1 tumors. The immunotherapy mixture did not affect tumor growth, while the combination with the TMA-ARB increased the time to reach 1,000 mm^3 by 77%, from 10 to 18 d ($P < 0.01$). $n = 8$–9. (*D*–*F*) Metastatic setting animal survival studies in mice with spontaneous lung metastases arising from orthotopic breast tumors treated with immune checkpoint blockers in combination with the TMA-ARB. Following resection of the primary tumors to leave only the metastatic disease, mice were treated with the immune checkpoint blocker mixture and TMA-ARB using the above schedule. (*D*) Animal survival in mice with spontaneous metastases from E0771 primary tumors. The immunotherapy mixture did not extend animal survival, yet its combination with the TMA-ARB improved animal survival greatly versus the controls ($P = 0.022$) and the immunotherapy mixture alone ($P < 0.045$). $n = 6$–9. (*E*) Animal survival in mice with spontaneous metastases from MCa-M3C primary tumors. The immunotherapy mixture did not extend animal survival, yet its combination with the TMA-ARB improved animal survival by 195% versus the controls ($P < 0.01$) and by 151% versus the immunotherapy mixture alone ($P = 0.013$). $n = 11$–13. (*F*) Animal survival in mice with spontaneous metastases from 4T1 primary tumors. The immunotherapy mixture did not extend animal survival, meanwhile the combination with the TMA-ARB improved animal survival by 41% versus the controls ($P < 0.01$) and by 26% versus the immunotherapy mixture alone ($P = 0.0153$). $n = 9$.

TMA-ARBs Extend Animal Survival in Combination with Immune Checkpoint Blockers. Since the majority of breast cancer-related deaths occur due to metastatic disease, we tested whether the combination of the TMA-ARB with the immune checkpoint mixture improved animal survival in the metastatic setting. We implanted the breast cancer models E0771, MCa-M3C, and 4T1 in the primary (orthotopic) setting in syngeneic mice and then surgically resected these primary tumors once they reached a large size. After waiting 4 d (E0771 and MCa-M3C) or 2 d (4T1) following resection to allow the growth of metastases, we began treatment of the metastatic disease. We then assessed animal survival following one cycle of treatment (Fig. 4 *D–F* and *SI Appendix*, Fig. S22). Once again the TMA-ARB monotherapy did not affect animal survival. However, in this metastatic setting the immune checkpoint mixture of α-CTLA4 + α-PD-1 also had no effect on animal survival. In contrast, the combination of the TMA-ARB with the immune checkpoint mixture increased cure rates to 88% (versus 22% for controls; $P = 0.022$) for mice with metastatic E0771. Furthermore, this combination extended median survival by 195% (118 versus 40 d for controls; $P < 0.01$) for mice with metastatic MCa-M3C and by 41% (24 d versus 17 d for controls; $P < 0.01$) for mice with metastatic 4T1. Importantly, the combination resulted in cures in 45% of the mice with metastatic MCa-M3C, while the immune checkpoint mixture did not induce cures in this model. Furthermore, the TMA-ARB combined with the immune checkpoint mixture induced a long-term survival extension in 22 to 33% of the mice with metastatic 4T1. Thus, the TMA-ARB enhances immunotherapy outcomes in models of immunotherapy-refractory breast cancer.

Discussion

Based on our results we propose a model for how targeting angiotensin signaling can reprogram the immunosuppressive tumor microenvironment promoted by CAFs. CAF activity—proliferation and matrix production—compresses tumor blood vessels to cause low vascular perfusion and hypoxia (10). Here we show that the reduction in CAF activity by ARB or TMA-ARB treatment leads to vessel decompression as well as decreased TGF-β and hypoxia signaling, similar to our earlier findings (10, 19). Tumor TGF-β and hypoxia signaling can promote immunosuppression by increasing regulatory T lymphocyte function (15) and by driving exclusion of T lymphocytes from tumors (49, 50). These pathways can also promote CAF expression of CXCL13 (42), which is expressed by immunosuppressive CAFs (3) and can suppress T lymphocyte infiltration deep into tumors via B lymphocytes (6). Our data suggest that reprogramming CAFs with ARB or TMA-ARB treatment can decrease their immunosuppressive CXCL13 production. Angiotensin signaling can also recruit protumor macrophages to tumors (38). Our data also indicate that blocking this signaling increases the fraction of macrophage population that is more M1-like (antitumor). These broad immunostimulatory shifts result in more active and infiltrative cytotoxic T lymphocytes in ARB- or TMA-ARB–treated tumors. Hence, the combination of the TMA-ARB and immune checkpoint blockers displays enhanced efficacy and better outcomes in both primary and metastatic breast tumors, where these immunosuppressive mechanisms may be similar.

Importantly, the effects of the TMA-ARB on the tumor microenvironment are greater than those of the free ARB. Thus, the TMA-ARB had a particularly large effect on outcomes for immune checkpoint blockers. Our data suggest that this is a result of reprogramming the immunosuppressive CAFs and microenvironment into an immunostimulatory state as well as converting CAFs to a less active and hypoxia-promoting state. Notably, the ARBs had no direct antitumor effects. We expect that, as is the case with many immunomodulatory therapies, ARBs must still be combined with immune checkpoint blockers or cytotoxic therapies to have significant antitumor effects. ARBs themselves neither promote cancer progression nor limit it through their CAF-reprogramming properties or other effects, in contrast to the potential deleterious effects of CAF depletion (16, 39). This may suggest that the CAF-reprogramming effects of ARBs are somewhat specific to inhibition of the protumor effects of CAFs. Indeed, the fact that ARBs promote antitumor immunity could be explained by selective activity in immunosuppressive CAFs or on immunosuppressive pathways. Regardless, ARBs can clearly improve the immune response to cancer across multiple breast cancer models. Other CAF-reprogramming agents may have similar effects and should be explored as well, possibly in formulations that improve their effectiveness.

Our data demonstrate that agents that have been repurposed for use in cancer can be redesigned with tumor-targeting properties to achieve greater efficacy. A similar strategy can be employed for many other types of anticancer agents to enhance their tumor-specific activity. Agents like ARBs, which are administered at slightly subtherapeutic doses, are likely to benefit the most from this strategy—as opposed to cytotoxics, which require increases in dosing by orders of magnitude to see improved responses. Still, these enhanced agents can lead to many previously undiscovered effects as shown here. The promise of TMA-ARBs for enhancing cancer immunotherapy outcomes through CAF and microenvironmental reprogramming warrants efforts toward clinical translation.

Materials and Methods

MCa-M3C cells (*Her2+*) were provided by P.H. and were isolated from lung metastases of mammary adenocarcinomas in mice generating spontaneous mammary tumors (*MMTV-PyVT*) (51). Orthotopic breast tumors were generated by implanting a small piece (1 mm^3) of viable tumor tissue (from a source tumor in a separate animal) into the mammary fat pad of a 6- to 8-wk-old female FVB (MCa-M3C model), BALB/c (4T1 model, *triple-negative*), or C57BL/6 (E0771 model, *triple-negative*) mouse. AK4.4 cells ($Kras^{G12D}$ *and* $p53^{+/-}$) were provided by Nabeel Bardeesy, Massachusettts General Hospital, Boston, MA, and were isolated from mice generating spontaneous pancreatic tumors (*Ptf1-Cre/LSL-*$Kras^{G12D}$*/*$p53^{Lox/+}$) (10). Orthotopic pancreatic tumors were similarly generated by implanting a small piece (1 mm^3) of viable tumor tissue into the pancreas of a 6- to 8-wk-old male FVB (AK4.4 model) mouse. For metastatic breast cancer models, mice bearing orthotopic E0771, MCa-M3C, or 4T1 breast tumors were allowed to progress until the point when 100% developed spontaneous lung tumors, which occurred once the primary tumors reached a large size (1,000 mm^3 in E0771 and MCa-M3C and 180 mm^3 in 4T1). The primary tumors were surgically excised at this tumor size to leave only the metastatic disease. All animal procedures were carried out following the Public Health Service Policy on Humane Care of Laboratory Animals and approved by the Institutional Animal Care and Use Committee of Massachusetts General Hospital. The data are presented as means with SEs. Groups were compared using an unpaired Student's *t* test, except for animal survival studies where a log-rank test was used. In pairwise comparisons within studies where multiple comparisons were made, *P* values were adjusted using Holm–Bonferroni correction. Experimental procedures are described in detail in *SI Appendix*.

ACKNOWLEDGMENTS. We thank Julia Kahn, Sylvie Roberge, and Carolyn Smith for technical assistance; Rakesh Ramjiawan and Nabeel Bardeesy for providing us with MCa-M3C and AK4.4 cells; and Eleanor Ager, Alan Crane, Dan Duda, Dai Fukumura, Jelena Grahovac, Timothy Padera, Mikael Pittet, and Trupti Vardam for helpful input. This work was supported by a Dana-Farber Harvard Cancer Center/MIT Koch Institute Bridge Project grant; a grant from the Lustgarten Foundation; a grant from the Ludwig Center at Harvard; National Cancer Institute Grants P01-CA080124, R01-CA126642, R01-CA085140, R01-CA115767, R01-CA098706, R01CA208205, U01CA224173, and R35CA197743; and US Department of Defense Breast Cancer Research Program Innovator Award W81XWH-10-1-0016. V.P.C. is a Fellow of the Life Sciences Research Foundation and was supported by Ruth L. Kirschstein NRSA Postdoctoral Fellowship T32-CA073479 from the NIH and by a Misrock Postdoctoral Fellowship from the Misrock Foundation through the S. Leslie Misrock (1949) Frontier Research Fund for Cancer Nanotechnology. I.X.C. was supported by a Gates Graduate Fellowship. M.R.N was supported by US Department of Defense Breast Cancer Research Program Postdoctoral Fellowship W81XWH-14-1-0034.

1. Topalian SL, Taube JM, Anders RA, Pardoll DM (2016) Mechanism-driven biomarkers to guide immune checkpoint blockade in cancer therapy. *Nat Rev Cancer* 16:275–287.
2. Chen DS, Mellman I (2017) Elements of cancer immunity and the cancer-immune set point. *Nature* 541:321–330.
3. Costa A, et al. (2018) Fibroblast heterogeneity and immunosuppressive environment in human breast cancer. *Cancer Cell* 33:463–479.e10.
4. Kraman M, et al. (2010) Suppression of antitumor immunity by stromal cells expressing fibroblast activation protein-alpha. *Science* 330:827–830.
5. Feig C, et al. (2013) Targeting CXCL12 from FAP-expressing carcinoma-associated fibroblasts synergizes with anti-PD-L1 immunotherapy in pancreatic cancer. *Proc Natl Acad Sci USA* 110:20212–20217.
6. Shalapour S, et al. (2015) Immunosuppressive plasma cells impede T-cell-dependent immunogenic chemotherapy. *Nature* 521:94–98.
7. Chen IX, et al. (2019) Blocking CXCR4 alleviates desmoplasia, increases T-lymphocyte infiltration, and improves immunotherapy in metastatic breast cancer. *Proc Natl Acad Sci USA* 116:4558–4566.
8. Salmon H, et al. (2012) Matrix architecture defines the preferential localization and migration of T cells into the stroma of human lung tumors. *J Clin Invest* 122:899–910.
9. Chauhan VP, et al. (2014) Compression of pancreatic tumor blood vessels by hyaluronan is caused by solid stress and not interstitial fluid pressure. *Cancer Cell* 26:14–15.
10. Chauhan VP, et al. (2013) Angiotensin inhibition enhances drug delivery and potentiates chemotherapy by decompressing tumour blood vessels. *Nat Commun* 4:2516.
11. Stylianopoulos T, et al. (2012) Causes, consequences, and remedies for growth-induced solid stress in murine and human tumors. *Proc Natl Acad Sci USA* 109: 15101–15108.
12. Barsoum IB, Smallwood CA, Siemens DR, Graham CH (2014) A mechanism of hypoxia-mediated escape from adaptive immunity in cancer cells. *Cancer Res* 74:665–674.
13. Calcinotto A, et al. (2012) Modulation of microenvironment acidity reverses anergy in human and murine tumor-infiltrating T lymphocytes. *Cancer Res* 72:2746–2756.
14. Noman MZ, et al. (2014) PD-L1 is a novel direct target of HIF-1α, and its blockade under hypoxia enhanced MDSC-mediated T cell activation. *J Exp Med* 211:781–790.
15. Facciabene A, et al. (2011) Tumour hypoxia promotes tolerance and angiogenesis via CCL28 and T(reg) cells. *Nature* 475:226–230.
16. Özdemir BC, et al. (2014) Depletion of carcinoma-associated fibroblasts and fibrosis induces immunosuppression and accelerates pancreas cancer with reduced survival. *Cancer Cell* 25:719–734.
17. Sherman MH, et al. (2014) Vitamin D receptor-mediated stromal reprogramming suppresses pancreatitis and enhances pancreatic cancer therapy. *Cell* 159:80–93.
18. Jain RK (2014) Antiangiogenesis strategies revisited: From starving tumors to alleviating hypoxia. *Cancer Cell* 26:605–622.
19. Diop-Frimpong B, Chauhan VP, Krane S, Boucher Y, Jain RK (2011) Losartan inhibits collagen I synthesis and improves the distribution and efficacy of nanotherapeutics in tumors. *Proc Natl Acad Sci USA* 108:2909–2914.
20. Nakai Y, et al. (2013) A multicenter phase II trial of gemcitabine and candesartan combination therapy in patients with advanced pancreatic cancer: GECA2. *Invest New Drugs* 31:1294–1299.
21. Murphy JE, et al. (2018) Potentially curative combination of TGF-b1 inhibitor losartan and FOLFIRINOX (FFX) for locally advanced pancreatic cancer (LAPC): R0 resection rates and preliminary survival data from a prospective phase II study. *J Clin Oncol* 36: 4116.
22. Xia T, et al. (2018) Losartan loaded liposomes improve the antitumor efficacy of liposomal paclitaxel modified with pH sensitive peptides by inhibition of collagen in breast cancer. *Pharm Dev Technol* 23:13–21.
23. Helmlinger G, Yuan F, Dellian M, Jain RK (1997) Interstitial pH and pO2 gradients in solid tumors in vivo: High-resolution measurements reveal a lack of correlation. *Nat Med* 3:177–182.
24. Thistlethwaite AJ, Leeper DB, Moylan Iii DJ, Nerlinger RE (1985) pH distribution in human tumors. *Int J Radiat Oncol Biol Phys* 11:1647–1652.
25. Wike-Hooley JL, van den Berg AP, van der Zee J, Reinhold HS (1985) Human tumour pH and its variation. *Eur J Cancer Clin Oncol* 21:785–791.
26. Yatvin MB, Kreutz W, Horwitz BA, Shinitzky M (1980) pH-sensitive liposomes: Possible clinical implications. *Science* 210:1253–1255.
27. Zhu L, Torchilin VP (2013) Stimulus-responsive nanopreparations for tumor targeting. *Integr Biol* 5:96–107.
28. Cheng CJ, et al. (2015) MicroRNA silencing for cancer therapy targeted to the tumour microenvironment. *Nature* 518:107–110.
29. Murthy N, Thng YX, Schuck S, Xu MC, Fréchet JMJ (2002) A novel strategy for encapsulation and release of proteins: Hydrogels and microgels with acid-labile acetal cross-linkers. *J Am Chem Soc* 124:12398–12399.
30. Heffernan MJ, Murthy N (2005) Polyketal nanoparticles: A new pH-sensitive biodegradable drug delivery vehicle. *Bioconjug Chem* 16:1340–1342.
31. Yang SC, Bhide M, Crispe IN, Pierce RH, Murthy N (2008) Polyketal copolymers: A new acid-sensitive delivery vehicle for treating acute inflammatory diseases. *Bioconjug Chem* 19:1164–1169.
32. Lynn DM, Anderson DG, Putnam D, Langer R (2001) Accelerated discovery of synthetic transfection vectors: Parallel synthesis and screening of a degradable polymer library. *J Am Chem Soc* 123:8155–8156.
33. Anderson DG, Lynn DM, Langer R (2003) Semi-automated synthesis and screening of a large library of degradable cationic polymers for gene delivery. *Angew Chem Int Ed Engl* 42:3153–3158.
34. Cabral H, et al. (2011) Accumulation of sub-100 nm polymeric micelles in poorly permeable tumours depends on size. *Nat Nanotechnol* 6:815–823.
35. Chauhan VP, et al. (2012) Normalization of tumour blood vessels improves the delivery of nanomedicines in a size-dependent manner. *Nat Nanotechnol* 7:383–388.
36. Liu B, Thayumanavan S (2017) Substituent effects on the pH sensitivity of acetals and ketals and their correlation with encapsulation stability in polymeric nanogels. *J Am Chem Soc* 139:2306–2317.
37. Incio J, et al. (2016) Obesity-induced inflammation and desmoplasia promote pancreatic cancer progression and resistance to chemotherapy. *Cancer Discov* 6:852–869.
38. Cortez-Retamozo V, et al. (2013) Angiotensin II drives the production of tumor-promoting macrophages. *Immunity* 38:296–308.
39. Pinter M, Jain RK (2017) Targeting the renin-angiotensin system to improve cancer treatment: Implications for immunotherapy. *Sci Transl Med* 9:eaan5616.
40. Liu H, et al. (2017) Use of angiotensin system inhibitors is associated with immune activation and longer survival in nonmetastatic pancreatic ductal adenocarcinoma. *Clin Cancer Res* 23:5959–5969.
41. Motz GT, et al. (2014) Tumor endothelium FasL establishes a selective immune barrier promoting tolerance in tumors. *Nat Med* 20:607–615.
42. Ammirante M, Shalapour S, Kang Y, Jamieson CAM, Karin M (2014) Tissue injury and hypoxia promote malignant progression of prostate cancer by inducing CXCL13 expression in tumor myofibroblasts. *Proc Natl Acad Sci USA* 111:14776–14781.
43. Tzachanis D, et al. (2001) Tob is a negative regulator of activation that is expressed in anergic and quiescent T cells. *Nat Immunol* 2:1174–1182.
44. Huang Y, et al. (2012) Vascular normalizing doses of antiangiogenic treatment reprogram the immunosuppressive tumor microenvironment and enhance immunotherapy. *Proc Natl Acad Sci USA* 109:17561–17566.
45. Tumeh PC, et al. (2014) PD-1 blockade induces responses by inhibiting adaptive immune resistance. *Nature* 515:568–571.
46. Wei SC, et al. (2017) Distinct cellular mechanisms underlie anti-CTLA-4 and anti-PD-1 checkpoint blockade. *Cell* 170:1120–1133.e17.
47. Fourcade J, et al. (2010) Upregulation of Tim-3 and PD-1 expression is associated with tumor antigen-specific CD8+ T cell dysfunction in melanoma patients. *J Exp Med* 207: 2175–2186.
48. Boutros C, et al. (2016) Safety profiles of anti-CTLA-4 and anti-PD-1 antibodies alone and in combination. *Nat Rev Clin Oncol* 13:473–486.
49. Mariathasan S, et al. (2018) TGFβ attenuates tumour response to PD-L1 blockade by contributing to exclusion of T cells. *Nature* 554:544–548.
50. Tauriello DVF, et al. (2018) TGFβ drives immune evasion in genetically reconstituted colon cancer metastasis. *Nature* 554:538–543.
51. Nia HT, et al. (2016) Solid stress and elastic energy as measures of tumour mechanopathology. *Nat Biomed Eng* 1:0004.